

## The high-pressure crystal chemistry of low albite and the origin of the pressure dependency of Al-Si ordering

R. T. DOWNS, R. M. HAZEN, L. W. FINGER

Geophysical Laboratory, Carnegie Institution of Washington, 5251 Broad Branch Road NW, Washington, DC 20015, U.S.A.

### ABSTRACT

Structural and volume compressibility data for low albite were obtained by single-crystal X-ray diffraction methods at pressures up to ~4 GPa. The bulk modulus was determined to be 54(1) GPa, with a pressure derivative of 6(1). Unit cell compression is anisotropic, as indicated by unit strain tensors. In the softest direction, approximately perpendicular to (100), the structure is three times more compressible than in the stiffest direction. Intensity data were collected, and structures were refined at 0.00, 0.44, 1.22, 2.68, and 3.78 GPa. With increasing pressure, (1) the volumes of the  $\text{TO}_4$  tetrahedra do not vary, (2) the volume of the  $\text{NaO}_7$  polyhedron varies linearly with the volume of the unit cell, and (3) Si-O-Si angles increase or remain constant, but only Al-O-Si angles decrease, which is consistent with the smaller force constant of the Al-O-Si vs. Si-O-Si angle. We conclude that compression is accomplished through the bending of Al-O-Si angles, which squeezes together the chains of four-membered rings that run parallel to [001] and that are separated by zigzag channels containing Na atoms. The feldspar three-dimensional tetrahedral framework can be considered to be made up of these chains, which are linked together by  $\text{O}_c$ -type atoms. The average value of the T- $\text{O}_c$ -T angle correlates with bulk moduli of alkali feldspars. Al-Si disorder tends to stiffen the T- $\text{O}_c$ -T angle in high albite, which in turn decreases the compressibility and thus can serve as a mechanism for pressure-dependent ordering of high to low albite.

### INTRODUCTION

The feldspar group of tetrahedral-framework aluminosilicates comprises ~60% of the total volume of the Earth's crust. Indeed, it might be possible to characterize the Earth's crust in terms of the pressure-temperature stability field of the feldspars. With increasing temperature and pressure these structures become unstable, and new structures are formed that contain  $\text{AlO}_6$  octahedra instead of  $\text{AlO}_4$  tetrahedra. The stability boundary of albite,  $\text{NaAlSi}_3\text{O}_8$ , has most recently been defined by Holland (1980) as  $P = 0.00265T(^{\circ}\text{C}) + 0.035$  (GPa), above which it transforms to jadeite + quartz. However, without high temperatures, the reaction appears to be quite slow, and the structure of albite is probably metastable at increasingly high pressures until it transforms to a glass phase. This pressure-induced amorphization has been observed for anorthite, another feldspar structure, through Raman (Daniel et al., 1993) and infrared (Williams and Jeanloz, 1989) spectral studies at 14–28 GPa.

Albite formed at lower temperatures displays complete ordering of the Al atom into one of four symmetrically nonequivalent, tetrahedrally coordinated cation sites; at higher temperatures, it may display complete disordering of Al into all four of the tetrahedral sites. A complete series exists between both forms that is defined by the degree of Al ordering. With the application of pressure and temperature, albite with specific degrees of order can

be synthesized (Martin, 1969; Goldsmith and Jenkins, 1985).

The structure of low albite has been extensively studied by single-crystal diffraction experiments at room conditions and at high and low temperatures (most recently: Armbruster et al., 1990; Smith et al., 1986; Wenk and Kroll, 1984; Harlow and Brown, 1980; Winter et al., 1977), with the major emphasis given to determining the nature of static vs. dynamic positional disorder at the Na site and on understanding Al-Si order-disorder systematics. The results of high- and low-temperature structure determinations have indicated that the Na atom is not statically disordered but instead vibrates with large anisotropic motion about a single center (Winter et al., 1977; Smith et al., 1986). The shape of the anisotropic thermal ellipsoid is completely determined by the positions of the coordinated O atoms, as demonstrated by a linear correlation between the mean-square displacement amplitudes of the Na atom toward the O atoms and by Na-O bond lengths.

Experimentally, Al-Si order-disorder is well documented, and its extent can be estimated within about 5% with X-ray diffraction techniques through the analysis of diffraction-peak positions [for example,  $\Delta 131 = 2\theta(131) - 2\theta(1\bar{3}1)$ ], cell parameters, or T-O bond lengths (Kroll and Ribbe, 1980; Kroll, 1983). However, the crystal-chemical reasons for the ordering of the Al atom into the T1O site are not well understood. The ionic argument is

that since the  $O_{A1}$  atom is bonded to two alkali cations, then one of its two tetrahedrally coordinated cations should include an Al atom for charge-balance considerations. The covalent argument suggests that because of  $\pi$  bonding effects, the Si-O-Si angles should be larger on average than Al-O-Si angles. Since the T- $O_{Bm}$ -T and T- $O_{Dm}$ -T angles are wider than  $150^\circ$ , then these O atoms should prefer bonding to Si atoms. This leaves only the T1O site for Al atoms (see Smith and Brown, 1988, for further discussion and references).

The compressibility of albite ( $K_0 = 48$  GPa) was first determined by Yoder and Weir (1951) using a piston-cylinder apparatus to define the reaction nepheline + albite = 2 jadeite. With this value of the bulk modulus to calibrate pressure, Hazen and Prewitt (1977) used single-crystal X-ray diffraction methods to determine the variations of the unit-cell parameters of low albite in a Merrill-Bassett miniature diamond-anvil pressure cell. They argued that if the large anisotropic displacements of the Na atom indicated static disorder, then the low albite structure might transform from  $C\bar{1}$  to  $P\bar{1}$  symmetry upon decrease in volume when the Na atoms order into two different sites, which is analogous to the transformation observed in anorthite. However, no transition was detected.

Angel et al. (1988) determined the comparative compressibilities of anorthite ( $CaAl_2Si_2O_8$ ), low albite, and high sanidine ( $KAlSi_3O_8$ ) by loading three crystals simultaneously into a Merrill-Bassett diamond-anvil pressure cell and using X-ray diffraction techniques to obtain unit-cell volumes at pressures up to 5 GPa. Low albite and high sanidine were reported to have similar compressibilities ( $K_0 = 70$  and 67 GPa, respectively), whereas anorthite was less compressible ( $K_0 = 94$  GPa) and underwent a phase transformation near 2.6 GPa. Hackwell and Angel (1992) also determined the compressibilities of reedmergnerite ( $NaBSi_3O_8$ ,  $K_0 = 69$  GPa) and danburite ( $CaB_2Si_2O_8$ ,  $K_0 = 114$  GPa) and reanalyzed the data of Angel et al. (1988), providing modified bulk moduli of 58 and 83 GPa for low albite and anorthite, respectively, while constraining the pressure derivative of the bulk modulus,  $K'_0$ , to a value of 4. The bulk modulus of microcline was determined by Hackwell (1993) to be 63 GPa ( $K'_0 = 4$ ), and evidence for a phase transition near 3.7 GPa was observed. These studies provide data for comparing the effects of M site (M = Na, K, Ca) diversity in the interstitial cavities of the negatively charged tetrahedral framework and for comparing different T-O-T linkages (T = Si, Al, B). Hackwell and Angel (1992) concluded that the most important contribution to the differences in compressibilities is that of stronger Ca<sup>2+</sup>-O vs. weaker Na<sup>1+</sup>-O and K<sup>1+</sup>-O bonds and stiffer B-O-Si vs. softer Al-O-Si and Si-O-Si bridging angles. The similar  $K_0$  values for low albite and high sanidine (with complete Al-Si disorder over the tetrahedral sites) suggest that there is little difference between Si-O-Si and Al-O-Si linkages.

The structure of anorthite was determined at 2.5 and

3.1 GPa (Angel, 1988) to examine the effects of pressure and the mechanism of the phase transition at 2.6 GPa. A major difficulty in collecting X-ray intensity data from single-crystal samples of triclinic symmetry that are confined in diamond-anvil cells is that much of reciprocal space is inaccessible because of the particular orientation of the sample and the shielding of the X-ray beam by the high-pressure cell. Angel (1988) attempted to overcome this problem by collecting one set of intensities with the crystal in a particular orientation and then reloading the pressure cell at the same pressure as before but with the crystal in a new orientation and collecting a second set of intensities. Angel combined the two data sets and refined the structure using a different scale factor for each data set at each pressure, but there were still correlation problems and so the data were refined assuming  $I\bar{1}$  symmetry. Tetrahedral bond lengths and volumes remained constant over the pressure interval, and only a few T-O-T angles changed. A calculation based on the reported data indicated that the average T-O-T angle,  $\langle T-O-T \rangle$ , varies as  $136.8(3) - 0.29(11)P$  (GPa). The longer Ca-O bonds show some compression, but the volume of the CaO<sub>7</sub> polyhedron did not decrease over the pressure interval. Angel (1988) concluded that the anorthite structure accommodates compression by the tilting of rigid tetrahedra and the bending of T-O-T angles into interstitial cavities occupied by Ca cations. Feldspar bulk moduli should thus be controlled by the stiffness of the T-O-T angles and the strength of the M-O bonds. For a more complete review of the effects of pressure on the feldspar group of minerals, the reader is referred to Angel (1994).

The present study includes the first determination of the structure of low albite as a function of pressure. In obtaining these data, we hoped to identify the structural mechanism for compression. In particular, as the tetrahedra are not expected to change much below 4 GPa, the role of the Na atom and its large site and the variations of the Si-O-Si and Al-O-Si angles should prove interesting.

## EXPERIMENTAL METHODS

### Structure refinement at room pressure

The albite crystal used in this study is from Crete and was kindly supplied by Paul Powhat of the Smithsonian Institution (specimen no. U.S.N.M. 123519). The sample, measuring  $90 \times 75 \times 40$   $\mu\text{m}$ , is a (001) cleavage fragment from a clear, gem-quality, 2.5-cm crystal. Another fragment from this particular specimen has also been used in a study of O diffusion by Giletti et al. (1978), who determined its chemical composition to be  $Ab_{99.3}An_{0.3}Or_{0.4}$ .

The room-pressure diffraction data were collected in air on a Rigaku AFC-5R diffractometer operated at 45 kV and 180 mA, with monochromatic MoK $\alpha$  radiation ( $\lambda = 0.7093$  Å). Selected reflection profiles were checked to verify crystal perfection and that twinning was not present. The crystal was confirmed to have space group

TABLE 1. A summary of the Crete low albite unit-cell data

| <i>P</i> (GPa) | <i>a</i> (Å) | <i>b</i> (Å) | <i>c</i> (Å) | $\alpha$ (°) | $\beta$ (°) | $\gamma$ (°) | <i>V</i> (Å <sup>3</sup> ) |
|----------------|--------------|--------------|--------------|--------------|-------------|--------------|----------------------------|
| 0.00*          | 8.1372(6)    | 12.7867(15)  | 7.1574(6)    | 94.245(9)    | 116.605(6)  | 87.809(9)    | 664.02(9)                  |
| 0.44*          | 8.1104(13)   | 12.7710(15)  | 7.1482(21)   | 94.244(29)   | 116.667(14) | 87.835(19)   | 659.82(21)                 |
| 0.65           | 8.0924(12)   | 12.7577(6)   | 7.1394(22)   | 94.253(13)   | 116.714(14) | 87.852(9)    | 656.58(21)                 |
| 1.22*          | 8.0510(16)   | 12.7336(5)   | 7.1242(22)   | 94.252(10)   | 116.784(17) | 87.909(7)    | 650.21(22)                 |
| 1.47           | 8.0334(21)   | 12.7235(16)  | 7.1172(29)   | 94.251(29)   | 116.886(22) | 87.925(22)   | 647.17(29)                 |
| 1.80           | 8.0154(18)   | 12.7109(14)  | 7.1099(45)   | 94.232(28)   | 116.921(24) | 87.930(18)   | 644.12(42)                 |
| 2.07           | 7.9928(26)   | 12.6995(11)  | 7.1021(40)   | 94.239(25)   | 116.941(28) | 87.971(18)   | 640.90(39)                 |
| 2.38           | 7.9790(16)   | 12.6908(10)  | 7.0928(42)   | 94.222(20)   | 116.943(22) | 87.991(13)   | 638.52(38)                 |
| 2.68*          | 7.9567(21)   | 12.6784(10)  | 7.0897(37)   | 94.217(21)   | 116.992(24) | 88.025(15)   | 635.56(35)                 |
| 3.13           | 7.9295(18)   | 12.6627(8)   | 7.0808(29)   | 94.183(18)   | 117.025(20) | 88.056(12)   | 631.66(28)                 |
| 3.44           | 7.9143(14)   | 12.6538(9)   | 7.0720(33)   | 94.180(18)   | 117.046(18) | 88.085(12)   | 629.09(30)                 |
| 3.78*          | 7.8925(17)   | 12.6400(15)  | 7.0667(39)   | 94.177(29)   | 117.074(21) | 88.128(19)   | 626.06(36)                 |
| 3.92           | 7.8836(24)   | 12.6359(13)  | 7.0650(32)   | 94.179(26)   | 117.071(25) | 88.136(18)   | 625.02(31)                 |
| 4.05           | 7.8738(17)   | 12.6314(15)  | 7.0628(17)   | 94.169(30)   | 117.064(17) | 88.144(21)   | 623.87(19)                 |

\* Intensity data were collected at these pressures.

symmetry  $C\bar{1}$ , with cell dimensions  $a = 8.1372(6)$ ,  $b = 12.7867(15)$ ,  $c = 7.1574(6)$  Å,  $\alpha = 94.245(9)$ ,  $\beta = 116.605(6)$ , and  $\gamma = 87.809(9)^\circ$ , and a cell volume of 664.02(9) Å<sup>3</sup> (Table 1). These values agree with those determined in previous studies of other ordered low-albite crystals (Armbruster et al., 1990; Wenk and Kroll, 1984; Harlow and Brown, 1980; Wainwright and Starkey, 1968). Cell parameters are sensitive indicators of Al-Si order, so we conclude that this crystal is a representative sample of ordered low albite.

A hemisphere of intensity data,  $I_{hkl}$ , was collected to  $(\sin \theta)/\lambda = 0.7$  Å<sup>-1</sup> from a total of 1932 symmetrically distinct reflections. No absorption correction was applied to the intensities because the linear-absorption coefficient is sufficiently small ( $\mu_L = 9.00$  cm<sup>-1</sup>). Neutral atomic scattering factors (Doyle and Turner, 1968), as well as real and imaginary anomalous dispersion corrections, were used to model the electron distribution. We refined the structure with anisotropic displacement factors and type 2 isotropic extinction (Becker and Coppens, 1975) to  $R = 0.031$  and  $R_w = 0.034$  using a revised version of RFIN4 (Finger and Prince, 1975). The structure factors were weighted by  $[\sigma_F^2 + (pF)^2]^{-1}$ , where  $\sigma_F$  was obtained from counting statistics and  $p = 0.023$  was chosen to ensure that the errors were normally distributed through probability plot analysis (Abrahams and Keve, 1971;

Ibers and Hamilton, 1974). This procedure also ensures that  $\chi^2$  will be close to 1. The refined values of the positional and displacement parameters are listed in Table 2. They are in agreement with other room-condition refinements and particularly with model 9 of the Armbruster et al. (1990) study of the systematics of refinement procedures on low-albite crystals.

#### High-pressure lattice parameters

The crystal was transferred to a miniature diamond-anvil cell (modified after Merrill and Bassett, 1974) with a 4:1 methanol to ethanol mixture as a pressure medium. The pressure calibration was facilitated by fitting Lorentzian functions to the fluorescence spectra of several small ruby chips that were included in the diamond-anvil cell. From least-squares estimates of the ruby  $R_1$  and  $R_2$  peak positions, we determined the pressure of the experiment using the relationship established by Mao et al. (1978) with an error of approximately 0.05 GPa. The positions of 32 reflections in the range  $25^\circ \leq 2\theta \leq 40^\circ$  were recorded with the eight-reflection centering technique (King and Finger, 1979) on an automated Huber four-circle diffractometer using monochromatic MoK $\alpha$  radiation at 13 pressures up to 4.05 GPa. Above this pressure, the crystal became loose in the diamond cell, and reliable data could no longer be collected. A least-

TABLE 2. A summary of the Crete low albite structural data at room conditions

| Atom             | <i>x</i>    | <i>y</i>    | <i>z</i>    | $B_{eq}$ (Å <sup>2</sup> ) | $\beta_{11}$ | $\beta_{22}$ | $\beta_{33}$ | $\beta_{12}$ | $\beta_{13}$ | $\beta_{23}$ |
|------------------|-------------|-------------|-------------|----------------------------|--------------|--------------|--------------|--------------|--------------|--------------|
| Al <sub>10</sub> | 0.00887(8)  | 0.16835(4)  | 0.20845(8)  | 0.65(1)                    | 0.00334(9)   | 0.00102(3)   | 0.00386(11)  | -0.00025(4)  | 0.00183(8)   | 0.00008(4)   |
| Si <sub>1m</sub> | 0.00370(7)  | 0.82030(4)  | 0.23707(7)  | 0.60(1)                    | 0.00325(8)   | 0.00094(3)   | 0.00325(11)  | 0.00027(3)   | 0.00156(7)   | 0.00019(4)   |
| Si <sub>2o</sub> | 0.69161(7)  | 0.11020(4)  | 0.31483(8)  | 0.64(1)                    | 0.00299(8)   | 0.00082(3)   | 0.00442(11)  | 0.00000(3)   | 0.00152(7)   | 0.00018(4)   |
| Si <sub>2m</sub> | 0.68158(7)  | 0.88176(4)  | 0.36040(8)  | 0.63(1)                    | 0.00280(8)   | 0.00086(3)   | 0.00443(11)  | 0.00011(3)   | 0.00156(7)   | 0.00026(4)   |
| Na               | 0.26823(14) | 0.98930(9)  | 0.14611(17) | 2.89(2)                    | 0.00591(17)  | 0.00643(8)   | 0.01685(28)  | -0.00089(9)  | 0.00407(17)  | -0.00604(12) |
| O <sub>A1</sub>  | 0.00523(19) | 0.13114(11) | 0.96733(20) | 1.07(2)                    | 0.0071(3)    | 0.00163(8)   | 0.0049(3)    | -0.0000(1)   | 0.0034(2)    | 0.0005(1)    |
| O <sub>A2</sub>  | 0.59186(18) | 0.99705(10) | 0.28040(20) | 0.83(2)                    | 0.0036(2)    | 0.00100(7)   | 0.0060(3)    | -0.0001(1)   | 0.0014(2)    | 0.0004(1)    |
| O <sub>B0</sub>  | 0.81268(19) | 0.10974(11) | 0.19097(23) | 1.17(2)                    | 0.0056(2)    | 0.00178(8)   | 0.0086(3)    | -0.0006(1)   | 0.0043(2)    | -0.0003(1)   |
| O <sub>Bm</sub>  | 0.82013(19) | 0.85098(12) | 0.25848(24) | 1.39(2)                    | 0.0058(3)    | 0.00233(8)   | 0.0112(4)    | 0.0009(1)    | 0.0058(3)    | 0.0003(1)    |
| O <sub>C0</sub>  | 0.01288(19) | 0.30187(10) | 0.27091(22) | 1.03(2)                    | 0.0050(2)    | 0.00116(7)   | 0.0079(3)    | -0.0003(1)   | 0.0027(2)    | -0.0000(1)   |
| O <sub>Cm</sub>  | 0.02337(19) | 0.69355(10) | 0.22885(22) | 1.07(2)                    | 0.0046(2)    | 0.00108(7)   | 0.0082(3)    | 0.0004(1)    | 0.0018(2)    | 0.0004(1)    |
| O <sub>D0</sub>  | 0.20681(19) | 0.10907(10) | 0.38899(21) | 1.11(2)                    | 0.0054(2)    | 0.00172(8)   | 0.0048(3)    | 0.0005(1)    | 0.0011(2)    | 0.0004(1)    |
| O <sub>Dm</sub>  | 0.18403(20) | 0.86804(11) | 0.43600(22) | 1.26(2)                    | 0.0061(3)    | 0.00187(8)   | 0.0051(3)    | -0.0005(1)   | 0.0004(2)    | -0.0002(1)   |

Note:  $B_{eq}$  represents the isotropic equivalent of the anisotropic displacement factors given by  $\exp(-\sum \Sigma h_i h_j \beta_{ij})$ .

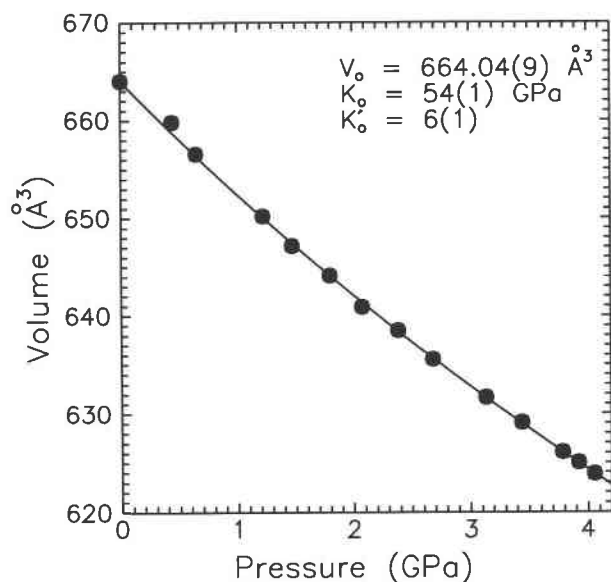


Fig. 1. The unit-cell volume of low albite as a function of pressure. The solid circles represent the experimental data from Table 1. The error in the pressure determination is estimated to be about 0.05 GPa, and the errors in the unit-cell volumes are smaller than the dimension of the dots. The solid line represents the weighted nonlinear best-fit curve for a third-order Birch-Murnaghan equation of state, with refined parameters as listed.

squares refinement of the diffraction data gave the cell dimensions in Table 1. The estimated errors of the *c*-cell edge are systematically larger than those of the *a*- and *b*-cell edges because the shape of the crystal fragment resulted in *c\** being aligned nearly parallel to the diamond-cell axis. As a consequence of this particular alignment, all the reflections closer than ~57° to *c\** were inaccessible during the entire experiment.

**Structure refinements at high pressures**

Intensity data for the low-albite crystal were recorded up to  $(\sin \theta)/\lambda = 0.7 \text{ \AA}^{-1}$  ( $2\theta \leq 60^\circ$ ) for refinements of the structure at 0.44, 1.22, 2.68, and 3.78 GPa on an automated Huber diffractometer with monochromatic MoK $\alpha$  radiation operated at 45 kV and 40 mA. We used  $\omega$  scans of 1° widths in steps of 0.020° and counting times of 8 s per step. At each pressure, several hundred peaks that violate the *C*-centered lattice condition were scanned. No significant intensities were observed. A summary of the intensity collection procedures and refinement results is provided in Table 3. The restricted access to much of reciprocal space caused by the shielding of the diamond cell, as well as the particular orientation of the crystal, prevented the refinement of anisotropic displacement parameters for all atoms except Na.

**RESULTS**

**Equation of state and unit-cell strain**

The weighted volume and pressure data of Table 1 were fitted to a nonlinear third-order Birch-Murnaghan equa-

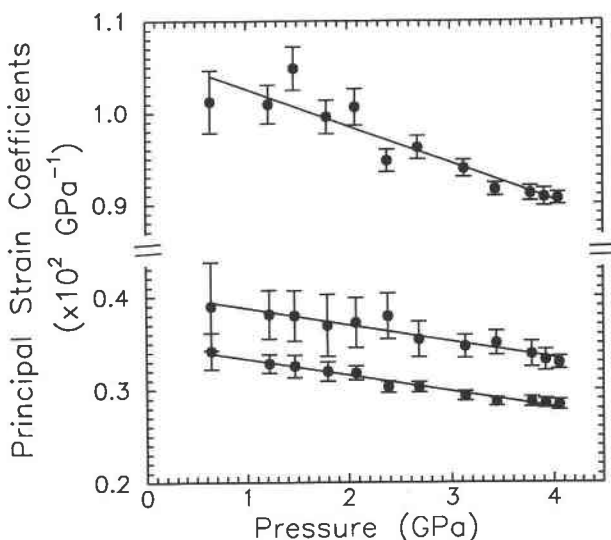


Fig. 2. The magnitudes of the principal unit-strain coefficients between room pressure and *P*, as a function of pressure calculated with the Strain program of Ohashi (Hazen and Finger, 1982). The bars represent 1 sd. The solid lines represent the best linear fits of the data:  $|\epsilon_1| = 0.0107(1) - 0.040(5)P$ ,  $|\epsilon_2| = 0.0041(1) - 0.018(5)P$ ,  $|\epsilon_3| = 0.0035(1) - 0.017(2)P$ . The major axes of the strain ellipsoid at 3.78 GPa are oriented 26, 82, and 91°, with respect to *a*, *b*, and *c*; 113, 109, and 15°; and 103, 21, and 75° for  $\epsilon_1$ ,  $\epsilon_2$ , and  $\epsilon_3$ , respectively.

tion of state that gave a zero pressure volume,  $V_0 = 664.06(9) \text{ \AA}^3$ , a zero pressure bulk modulus,  $K_0 = 54(1) \text{ GPa}$ , and its pressure derivative,  $K'_0 = 6(1)$ . The volume-compressibility curve obtained in the analysis is displayed in Figure 1, along with the data recorded for the crystal. The bulk modulus obtained in our analysis is somewhat smaller than that determined by Hackwell and Angel (1992) [ $K_0 = 57(2) \text{ GPa}$ ,  $K'_0 = 4$ ] from the low angle data ( $9^\circ \leq 2\theta \leq 17^\circ$ ) that had been previously recorded by Angel et al. (1988). However, if we also constrain  $K'_0$  to a value of 4.0, then we obtain  $V_0 = 664.01(9) \text{ \AA}^3$ , and  $K_0 = 56.8(4) \text{ GPa}$ , in agreement with the Hackwell and Angel (1992) value.

An examination of the data in Table 1 shows that the cell compression is quite anisotropic, with  $\Delta a/a_0 : \Delta b/b_0 : \Delta c/c_0 = 2.67:1:1.09$ . The interaxial angles also vary systematically with pressure, with  $d\alpha/dP = -0.022^\circ/\text{GPa}$ ,  $d\beta/dP = 0.114^\circ/\text{GPa}$ , and  $d\gamma/dP = 0.084^\circ/\text{GPa}$ . However, because albite is triclinic, these axial measures do not describe the anisotropic compression, which can be better represented with strain tensors. Unit-strain tensors were computed using the Strain program written by Ohashi (Hazen and Finger, 1982). The magnitudes of the principal strain coefficients are plotted in Figure 2 as a function of pressure. Lines representing least-square fits to the data are superimposed. The strain ellipsoid is almost prolate uniaxial, with two relatively stiff axes of magnitudes  $0.350(5)$  and  $0.405(14) \times 10^{-2} \text{ GPa}^{-1}$  and a softer one [ $1.066(13) \times 10^{-2} \text{ GPa}^{-1}$ ] that is approxi-

**TABLE 3.** Intensity collection and refinement results for Crete low albite as a function of pressure

| <i>P</i> (GPa)                              | 0.00*       | 0.44        | 1.22        | 2.68        | 3.78        |
|---|-------------|-------------|-------------|-------------|-------------|
| No. obs. / > 2 $\sigma$ <sub><i>i</i></sub> | 476         | 418         | 431         | 414         | 418         |
| <i>R</i> <sup>**</sup>                      | 0.044       | 0.045       | 0.050       | 0.057       | 0.057       |
| <i>R</i> <sub>w</sub>                       | 0.049       | 0.058       | 0.065       | 0.071       | 0.071       |
| Unweighted <i>R</i>                         | 0.035       | 0.056       | 0.060       | 0.065       | 0.067       |
| Al <sub>10</sub> <i>x</i>                   | 0.0089(3)   | 0.0086(5)   | 0.0072(5)   | 0.0058(6)   | 0.0041(6)   |
| <i>y</i>                                    | 0.16819(9)  | 0.1681(2)   | 0.1675(2)   | 0.1664(2)   | 0.1657(2)   |
| <i>z</i>                                    | 0.2076(7)   | 0.2086(12)  | 0.2068(13)  | 0.2065(13)  | 0.2056(13)  |
| <i>B</i> (iso)                              | 0.64(3)     | 0.66(4)     | 0.57(5)     | 0.60(5)     | 0.62(5)     |
| Si <sub>1m</sub> <i>x</i>                   | 0.0040(3)   | 0.0032(4)   | 0.0018(5)   | -0.0003(6)  | -0.0030(6)  |
| <i>y</i>                                    | 0.82043(8)  | 0.8204(1)   | 0.8209(2)   | 0.8206(2)   | 0.8204(2)   |
| <i>z</i>                                    | 0.2366(6)   | 0.2364(11)  | 0.2362(12)  | 0.2361(13)  | 0.2351(13)  |
| <i>B</i> (iso)                              | 0.63(3)     | 0.65(4)     | 0.54(4)     | 0.54(5)     | 0.60(5)     |
| Si <sub>2o</sub> <i>x</i>                   | 0.6922(3)   | 0.6915(5)   | 0.6909(7)   | 0.6873(8)   | 0.6845(7)   |
| <i>y</i>                                    | 0.11044(9)  | 0.1099(2)   | 0.1096(2)   | 0.1085(2)   | 0.1071(2)   |
| <i>z</i>                                    | 0.3159(8)   | 0.3159(13)  | 0.3169(15)  | 0.3114(16)  | 0.3074(14)  |
| <i>B</i> (iso)                              | 0.59(3)     | 0.58(4)     | 0.52(5)     | 0.49(5)     | 0.57(5)     |
| Si <sub>2m</sub> <i>x</i>                   | 0.6816(4)   | 0.6810(6)   | 0.6765(8)   | 0.6716(9)   | 0.6657(8)   |
| <i>y</i>                                    | 0.88179(9)  | 0.8818(2)   | 0.8813(2)   | 0.8802(2)   | 0.8792(2)   |
| <i>z</i>                                    | 0.3609(9)   | 0.3632(15)  | 0.3600(18)  | 0.3599(20)  | 0.3555(17)  |
| <i>B</i> (iso)                              | 0.61(3)     | 0.58(4)     | 0.56(5)     | 0.48(5)     | 0.53(5)     |
| Na <i>x</i>                                 | 0.2691(5)   | 0.2660(8)   | 0.2639(9)   | 0.2587(9)   | 0.2596(9)   |
| <i>y</i>                                    | 0.9890(2)   | 0.9896(3)   | 0.9907(4)   | 0.9930(4)   | 0.9940(3)   |
| <i>z</i>                                    | 0.1489(12)  | 0.1411(19)  | 0.1419(21)  | 0.1392(21)  | 0.1462(20)  |
| <i>B</i> <sub>eq</sub>                      | 3.0(4)      | 3.6(7)      | 4.2(7)      | 3.8(7)      | 2.4(6)      |
| β <sub>11</sub>                             | 0.0066(12)  | 0.0064(17)  | 0.0092(21)  | 0.0104(24)  | 0.0058(24)  |
| β <sub>22</sub>                             | 0.0064(2)   | 0.0063(3)   | 0.0058(3)   | 0.0048(3)   | 0.0047(3)   |
| β <sub>33</sub>                             | 0.0180(73)  | 0.0310(129) | 0.0482(134) | 0.0429(140) | 0.0186(131) |
| β <sub>12</sub>                             | -0.0010(3)  | -0.0015(6)  | -0.0007(6)  | -0.0001(6)  | -0.0007(6)  |
| β <sub>13</sub>                             | 0.0052(29)  | 0.0079(47)  | 0.0168(53)  | 0.0160(59)  | 0.0056(57)  |
| β <sub>23</sub>                             | -0.0059(7)  | -0.0068(13) | -0.0048(14) | -0.0044(14) | -0.0056(13) |
| O <sub>A1</sub> <i>x</i>                    | 0.0061(8)   | 0.0067(11)  | 0.0060(14)  | 0.0073(15)  | 0.0093(16)  |
| <i>y</i>                                    | 0.1317(2)   | 0.1315(4)   | 0.1311(4)   | 0.1292(5)   | 0.1274(5)   |
| <i>z</i>                                    | 0.96892(17) | 0.9689(27)  | 0.9701(31)  | 0.9674(32)  | 0.9684(33)  |
| <i>B</i> (iso)                              | 1.17(6)     | 1.10(10)    | 0.93(11)    | 0.90(12)    | 0.85(12)    |
| O <sub>A2</sub> <i>x</i>                    | 0.5916(6)   | 0.5896(10)  | 0.5850(11)  | 0.5810(12)  | 0.5778(13)  |
| <i>y</i>                                    | 0.9971(2)   | 0.9973(4)   | 0.9965(4)   | 0.9964(4)   | 0.9960(4)   |
| <i>z</i>                                    | 0.2790(15)  | 0.2794(25)  | 0.2768(25)  | 0.2824(26)  | 0.2805(24)  |
| <i>B</i> (iso)                              | 0.77(5)     | 0.72(9)     | 0.48(9)     | 0.68(11)    | 0.46(10)    |
| O <sub>B0</sub> <i>x</i>                    | 0.8137(7)   | 0.8119(11)  | 0.8102(13)  | 0.8079(14)  | 0.8079(14)  |
| <i>y</i>                                    | 0.1101(2)   | 0.1091(4)   | 0.1065(4)   | 0.1020(5)   | 0.0995(5)   |
| <i>z</i>                                    | 0.1950(15)  | 0.1914(26)  | 0.1886(28)  | 0.1840(30)  | 0.1853(28)  |
| <i>B</i> (iso)                              | 1.05(6)     | 0.99(10)    | 1.05(12)    | 0.99(12)    | 1.04(12)    |
| O <sub>Bm</sub> <i>x</i>                    | 0.8190(7)   | 0.8188(11)  | 0.8147(13)  | 0.8116(14)  | 0.8054(14)  |
| <i>y</i>                                    | 0.8509(2)   | 0.8510(4)   | 0.8503(5)   | 0.8492(5)   | 0.8484(5)   |
| <i>z</i>                                    | 0.2563(16)  | 0.2565(26)  | 0.2505(29)  | 0.2550(30)  | 0.2507(30)  |
| <i>B</i> (iso)                              | 1.19(6)     | 1.18(10)    | 1.24(11)    | 1.27(13)    | 1.31(12)    |
| O <sub>Co</sub> <i>x</i>                    | 0.0124(7)   | 0.0107(10)  | 0.0083(13)  | -0.0007(14) | -0.0066(13) |
| <i>y</i>                                    | 0.3018(2)   | 0.3015(4)   | 0.3010(4)   | 0.3002(5)   | 0.2992(5)   |
| <i>z</i>                                    | 0.2690(16)  | 0.2698(25)  | 0.2727(30)  | 0.2722(31)  | 0.2704(28)  |
| <i>B</i> (iso)                              | 0.96(6)     | 0.86(9)     | 0.86(11)    | 0.88(11)    | 0.85(11)    |
| O <sub>Cm</sub> <i>x</i>                    | 0.0233(7)   | 0.0244(11)  | 0.0215(13)  | 0.0193(14)  | 0.0167(14)  |
| <i>y</i>                                    | 0.6934(2)   | 0.6940(4)   | 0.6941(4)   | 0.6935(4)   | 0.6933(5)   |
| <i>z</i>                                    | 0.2275(15)  | 0.2332(27)  | 0.2282(28)  | 0.2240(30)  | 0.2222(28)  |
| <i>B</i> (iso)                              | 0.92(6)     | 1.02(9)     | 0.88(11)    | 0.78(11)    | 0.87(11)    |
| O <sub>Do</sub> <i>x</i>                    | 0.2064(9)   | 0.2032(15)  | 0.2104(19)  | 0.2114(23)  | 0.2124(20)  |
| <i>y</i>                                    | 0.1089(2)   | 0.1085(4)   | 0.1090(4)   | 0.1103(5)   | 0.1118(5)   |
| <i>z</i>                                    | 0.3863(23)  | 0.3777(35)  | 0.3911(41)  | 0.3863(47)  | 0.3877(41)  |
| <i>B</i> (iso)                              | 1.19(8)     | 1.25(13)    | 1.08(15)    | 1.32(18)    | 1.084(16)   |
| O <sub>Dm</sub> <i>x</i>                    | 0.1809(9)   | 0.1768(16)  | 0.1744(18)  | 0.1782(22)  | 0.1770(20)  |
| <i>y</i>                                    | 0.8680(3)   | 0.8668(5)   | 0.8667(5)   | 0.8681(6)   | 0.8694(5)   |
| <i>z</i>                                    | 0.4286(21)  | 0.4228(35)  | 0.4232(38)  | 0.4291(44)  | 0.4341(42)  |
| <i>B</i> (iso)                              | 1.44(7)     | 1.42(11)    | 1.39(13)    | 1.59(15)    | 1.34(13)    |

Note: *B*(iso) is in cubic ångströms.

\* From the constrained data set.

\*\* Weights were computed by  $\sigma = \sqrt{\sigma_i^2 + p^2 F^2}$ .

mately perpendicular to (100) at room pressure. The negative trends of the data in Figure 2 result from the stiffening of the structure with increasing pressure. The slopes in the two stiffest directions are statistically equal ( $-0.017 \text{ GPa}^{-2}$ ), whereas in the softest direction, the structure be-

comes stiffer at twice the rate ( $-0.040 \text{ GPa}^{-2}$ ). If the slopes remain constant and the structure does not undergo a transformation, then the compression is approximately isotropic at  $\sim 30 \text{ GPa}$ . Concurrent with the change in anisotropy, the strain ellipsoid also rotates counter-

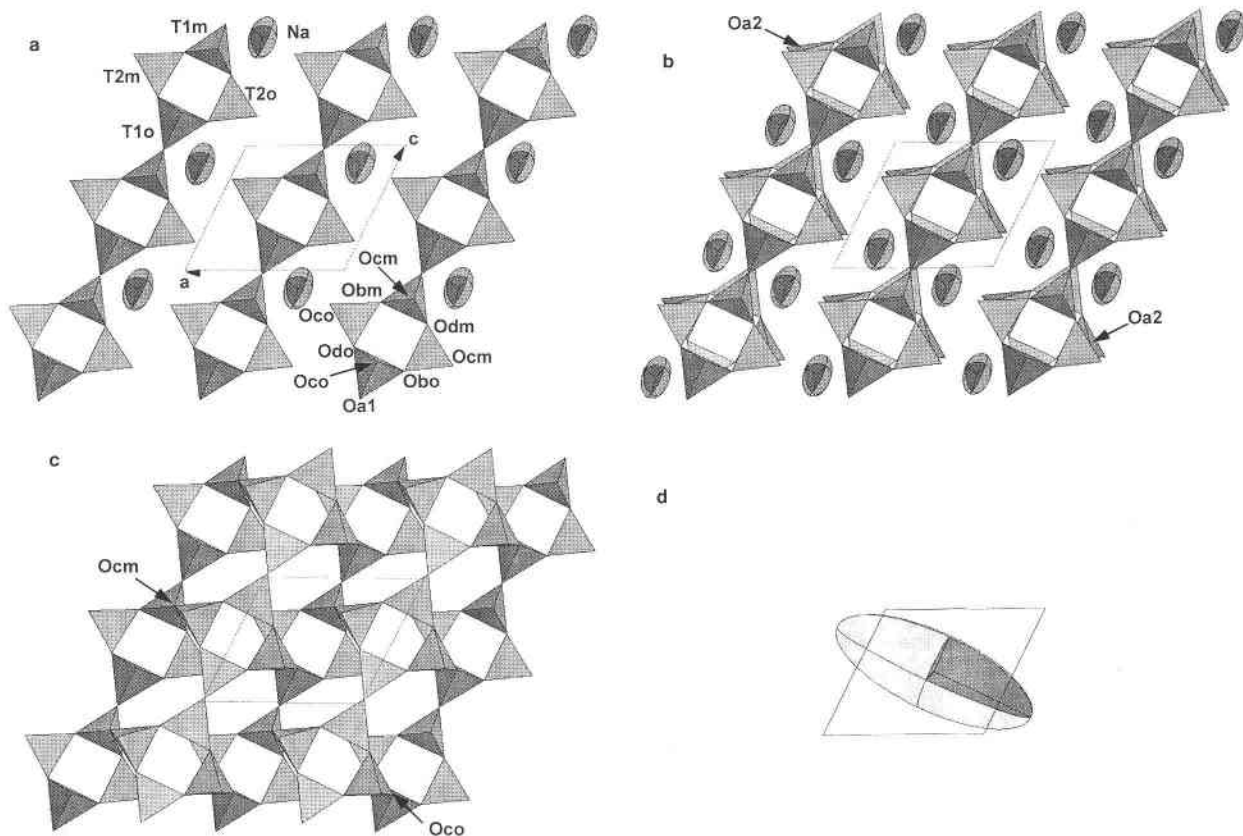


Fig. 3. (a) A representation of the chains of tetrahedra that are parallel to [001], with Na atoms shown as thermal ellipsoids in a slice of the albite structure,  $0.5 \leq y \leq 0.8$ . The view is down [010] with  $a$  and  $c$  as indicated. (b) This figure represents the slice  $0.3 \leq y \leq 0.8$  with the same orientation as a. We show the pairs of chains related by the inversion isometry and linked by means of the  $O_{A2}$  atoms. All the Na atoms are located between these layers of tetrahedral chains. (c) This figure represents the slice  $0.5 \leq y \leq 1.0$  with the same orientation as a. The layers

are linked by  $O_{Co}$  and  $O_{cm}$  atoms to form the double-crankshaft feature that runs along [100] and is commonly used to describe the feldspar structure. (d) The strain ellipsoid at 0–3.78 GPa and unit-cell outline. The magnitudes of the principal strains indicate that  $100\epsilon_1/(\epsilon_1 + \epsilon_2 + \epsilon_3) = 60\%$  of the volume decrease is due to compression along  $\epsilon_1$ , which is nearly perpendicular to (100). A comparison of the orientation of the strain ellipsoid and the crystal structure shows that compression is related to the soft zigzag channels that run parallel to [001].

clockwise around its most compressible axis by  $\sim 3.4^\circ$ /GPa. The unit-strain ellipsoid from 0 to 3.78 GPa is shown in Figure 3d, superimposed on an outline of the unit cell viewed along [010]. The orientation and anisotropy can be compared with the crystal structure illustrated in Figure 3a–3c.

### Structural variations with pressure

Selected bond lengths and angles are summarized in Table 4. The results of the refinement at room pressure are included in Table 4, along with the results provided from a subset of room-pressure structure factors that were restricted to the same set of reflections that were obtained at high pressure within the diamond cell. This procedure was considered necessary to provide a meaningful comparison of room-pressure and high-pressure results. Because of the particular orientation of the crystal within

the diamond-anvil cell, the bond lengths and angles calculated from the high-pressure data sets have large associated errors if they are oriented near  $c^*$ . Consequently, average  $TO_4$  bond lengths appear to be more meaningful than individual bond lengths within a given tetrahedron since the individual bond-length errors range from 0.001 to 0.03 Å.

A plot of the average T–O bond lengths for the four nonequivalent tetrahedra indicates that they appear to remain constant over the pressure range of the experiment (Fig. 4). The rigid behavior of the T–O bonds is not surprising, given the strength of the bond, the pressure range of the experiment, and the flexibility of the framework structure. Similar results have been observed for  $SiO_2$  framework structures refined at high pressures such as quartz and cristobalite (Hazen et al., 1989; Glinne-mann et al., 1992; Downs and Palmer, 1994) and for the  $AlO_4$  and  $SiO_4$  tetrahedra in the anorthite structure (An-

**TABLE 4.** Selected bond lengths and angles for Crete low albite as a function of pressure

| P (GPa)                                       | 0.00*      | 0.00**    | 0.44      | 1.22      | 2.68      | 3.78      |
|---|------------|-----------|-----------|-----------|-----------|-----------|
| $\langle \text{Al}_{10}\text{-O} \rangle$     | 1.7381(7)  | 1.734(4)  | 1.724(6)  | 1.733(7)  | 1.730(8)  | 1.725(7)  |
| $\langle \text{Si}_{1m}\text{-O} \rangle$     | 1.6108(7)  | 1.603(4)  | 1.588(6)  | 1.583(7)  | 1.589(8)  | 1.596(8)  |
| $\langle \text{Si}_{20}\text{-O} \rangle$     | 1.6156(7)  | 1.623(4)  | 1.632(6)  | 1.635(7)  | 1.622(7)  | 1.611(7)  |
| $\langle \text{Si}_{2m}\text{-O} \rangle$     | 1.6167(7)  | 1.623(4)  | 1.638(6)  | 1.615(7)  | 1.613(7)  | 1.609(7)  |
| $\text{Al}_{10}\text{-O}_{A1}\text{-Si}_{1m}$ | 141.44(9)  | 141.9(2)  | 141.9(4)  | 141.9(4)  | 140.8(5)  | 139.5(5)  |
| $\text{Si}_{20}\text{-O}_{A2}\text{-Si}_{2m}$ | 130.02(9)  | 129.7(4)  | 129.2(6)  | 128.5(6)  | 129.3(6)  | 130.1(6)  |
| $\text{Al}_{10}\text{-O}_{B0}\text{-Si}_{20}$ | 139.71(9)  | 141.1(6)  | 139.5(9)  | 137.6(10) | 135.2(11) | 135.4(9)  |
| $\text{Si}_{1m}\text{-O}_{Bm}\text{-Si}_{2m}$ | 161.18(11) | 160.2(7)  | 160.0(12) | 158.3(13) | 160.2(14) | 159.4(14) |
| $\text{Al}_{10}\text{-O}_{C0}\text{-Si}_{2m}$ | 129.65(9)  | 129.6(2)  | 129.4(3)  | 129.0(4)  | 126.3(4)  | 125.3(4)  |
| $\text{Si}_{1m}\text{-O}_{Cm}\text{-Si}_{20}$ | 135.74(9)  | 135.3(4)  | 136.8(6)  | 136.1(7)  | 136.7(8)  | 137.4(7)  |
| $\text{Al}_{10}\text{-O}_{D0}\text{-Si}_{2m}$ | 134.12(9)  | 133.7(4)  | 132.1(7)  | 134.5(8)  | 134.1(9)  | 135.5(8)  |
| $\text{Si}_{1m}\text{-O}_{Dm}\text{-Si}_{20}$ | 151.76(11) | 150.6(5)  | 150.9(8)  | 152.3(9)  | 152.1(9)  | 153.8(9)  |
| $\text{Na-O}_{A1}$                            | 2.538(2)   | 2.548(5)  | 2.534(8)  | 2.502(9)  | 2.460(9)  | 2.446(9)  |
| $\text{Na-O}_{A1}$                            | 2.665(2)   | 2.673(7)  | 2.634(9)  | 2.601(11) | 2.515(13) | 2.481(14) |
| $\text{Na-O}_{A2}$                            | 2.368(2)   | 2.362(5)  | 2.356(9)  | 2.319(9)  | 2.291(11) | 2.245(10) |
| $\text{Na-O}_{B0}$                            | 2.459(2)   | 2.498(11) | 2.431(19) | 2.406(21) | 2.349(20) | 2.382(19) |
| $\text{Na-O}_{C0}$                            | 2.977(2)   | 2.967(5)  | 2.981(7)  | 2.986(9)  | 2.984(10) | 2.963(9)  |
| $\text{Na-O}_{D0}$                            | 2.438(2)   | 2.414(10) | 2.400(16) | 2.419(19) | 2.366(20) | 2.332(17) |
| $\text{Na-O}_{Dm}$                            | 3.002(2)   | 2.958(11) | 2.983(17) | 2.980(18) | 2.981(20) | 2.963(19) |
| $V(\text{NaO}_7)$                             | 23.18      | 23.11     | 22.60     | 22.22     | 21.35     | 21.02     |

\* From the complete data set.

\*\* From the constrained data set.

gel, 1988). However, Levien and Prewitt (1981) reported that the Si-O bonds in coesite, the  $\text{SiO}_2$  structure that is most similar to the feldspar structure, appear to shorten by 0.006 Å with pressure up to 5.2 GPa. The  $\text{SiO}_4$  tetrahedral angles also do not appear to vary over the applied pressure range, with the tetrahedral angle variance (Robinson et al., 1971) remaining fairly constant ( $\sigma_{tet}^2 = 5-10$ ). On the other hand,  $\sigma_{tet}^2$  doubled from 20 at room pressure to 40 at 3.78 GPa for the  $\text{AlO}_4$  tetrahedron. The volumes of the tetrahedra do not appear to vary over the pressure range of the experiment.

The Na atom occupies an irregular interstitial cavity in

the negatively charged aluminosilicate framework. It is difficult to determine whether or not the M-site cation is coordinated to a given O atom in the alkali feldspars. In many structures, the M-O bond lengths display a broad range of values with no apparent distinguishable gaps. If  $M = \text{K}$  or  $\text{Rb}$ , then the coordination number is usually chosen as nine, but for  $M = \text{Li}$ , the coordination appears to be five (Smith and Brown, 1988). When  $M = \text{Na}$ , the coordination appears to depend, in part, on the framework cations. For  $\text{NaAlGe}_3\text{O}_8$  and  $\text{NaGaGe}_3\text{O}_8$ , there are four O atoms with short M-O bond lengths ( $\approx 2.4$  Å), and

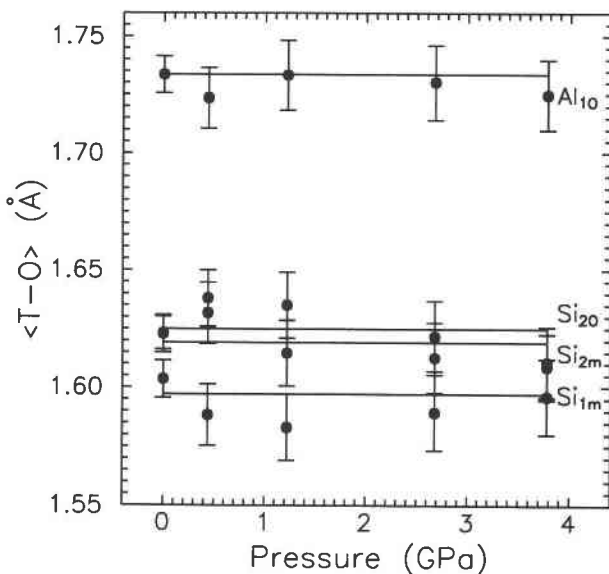


Fig. 4. The average T-O bond length for each of the four nonequivalent  $\text{TO}_4$  tetrahedra as a function of pressure. The error bars represent 1 sd, and horizontal lines are drawn to indicate that there is no significant change in bond length with pressure.

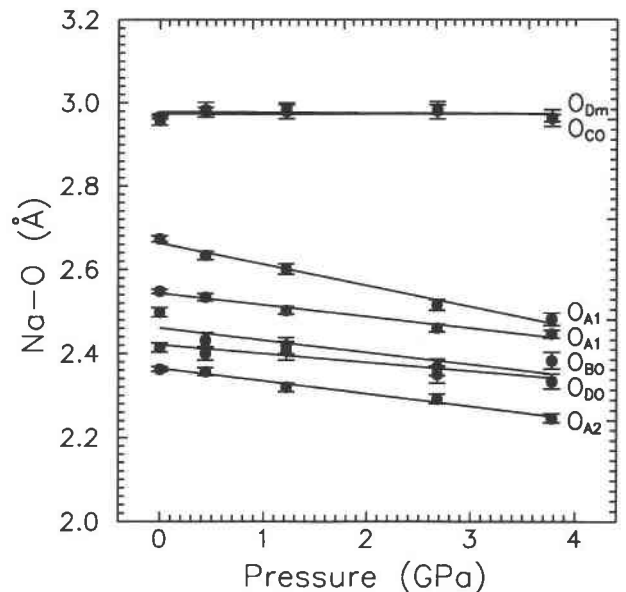


Fig. 5. The variation of Na-O bond length with pressure. The data are indicated by bars of 1 sd, and the lines represent least-squares linear fits to the data. Note that only the five shortest bonds show any changes.

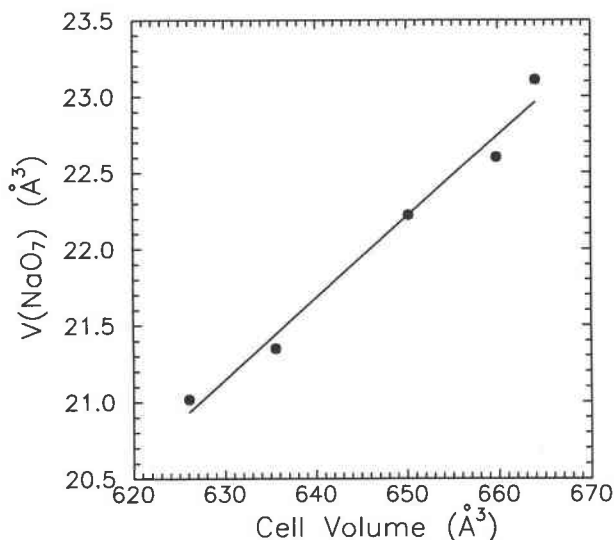


Fig. 6. The variation of the volume of the Na polyhedron with the volume of the unit cell. The best-fit linear equation is represented by the line.

for reedmergnerite,  $\text{NaBSi}_3\text{O}_8$ , there are five. Traditionally, mineralogists have chosen seven or nine as the coordination number of Na in albite. In this paper, we assume that the coordination number is seven in spite of the observation that with increasing pressure the two longer Na-O bonds ( $\sim 3.0$  Å) did not change in length, whereas the five shorter ones showed compression (Table 4, Fig. 5). These trends are different from those observed for anorthite (Angel, 1988), where only the longer Ca-O bonds showed compression and the  $\text{CaO}_7$  polyhedral volumes remained constant. This difference in behavior probably relates to the comparatively greater strength of the Ca-O bonds. The volume of the  $\text{NaO}_7$  polyhedron varies linearly with the volume of the unit cell (Fig. 6), with the bulk modulus of the  $\text{NaO}_7$  polyhedron calculated as  $K_0 = 26(2)$  GPa. The compression of the four  $\text{NaO}_7$  polyhedra accounts for 22% of the change in unit-cell volume.

Low albite contains eight nonequivalent O atoms, each associated with a bridging T-O-T angle. Variations of T-O-T angles with pressure are plotted in Figure 7. Only Al-O-Si angles showed a decrease with increasing pressure. In a molecular-orbital study of the bonding energetics in framework molecular sieves, Nicholas et al. (1992) derived potential energy curves for Al-O-Si and Si-O-Si angles in structural analogues of the disiloxane molecule, with high-level basis sets that included multiple polarization functions. They showed that the Al-O-Si angle, with a quadratic force constant of  $8.95$  kcal/(mol·rad<sup>2</sup>), is twice as soft in this molecule as the Si-O-Si angle, with a quadratic force constant of  $17.34$  kcal/(mol·rad<sup>2</sup>). The observation that only Al-O-Si angles decrease with pressure in low albite appears to be consistent with the molecular orbital calculations. On the other hand, this observation is not consistent with the Hackwell and An-

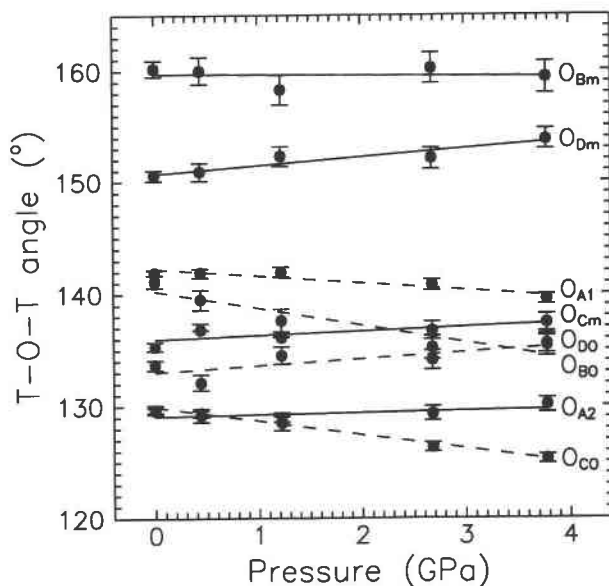


Fig. 7. The variation of the T-O-T angles with pressure. Error bars indicate 1 sd. Best-fit lines are superimposed: solid lines represent Si-O-Si angles and dashed lines represent Al-O-Si angles. The O atom involved in the angle is indicated. Note that only Al-O-Si angles decrease with increasing pressure.

gel (1992) conclusion that there is no difference between Al-O-Si and Si-O-Si angle bending behavior in feldspars at high pressure. However, the only structural data available to them were from anorthite, in which every angle is an Al-O-Si angle. Finally, given that there is little significant difference between the shape and orientation of the strain ellipsoids for high sanidine and low albite (Angel et al., 1988), it appears that differential T-O-T angle bending is not responsible for the shape and orientation of these ellipsoids. However, we show that it may be responsible for the difference in the sizes of these ellipsoids.

The average T-O-T angle, with a rate of  $-0.23(6)^\circ/\text{GPa}$ , barely decreases with pressure. This behavior is quite different from the compressional behavior of the silica polymorphs. In their study of the behavior of cristobalite with pressure, Downs and Palmer (1994) showed that  $V/V_0$  varies linearly with the normalized average Si-O-Si angle for quartz, cristobalite, and coesite. Clearly, the mechanism for compression in albite, even though it is a framework silicate, is quite different from that in the silica polymorphs. On the other hand, the T-O-T angle-bending rate in albite is statistically equal to the rate calculated for anorthite from the data of Angel (1988) [ $-0.29(11)^\circ/\text{GPa}$ ]. The average Al-O-Si angle in low albite varies with pressure as  $\langle \text{Al-O-Si} \rangle = 136.4(2) - 0.70(11)P$ . The significantly lower rate in anorthite is probably due to the different influences of the M cations on the bridging O atoms. The shorter and stronger  $\text{Ca}^{2+}\text{-O}_{\text{br}}$  bonds tend to stiffen the Al-O-Si angles, compared with the longer and weaker  $\text{Na}^{+}\text{-O}_{\text{br}}$  bonds.

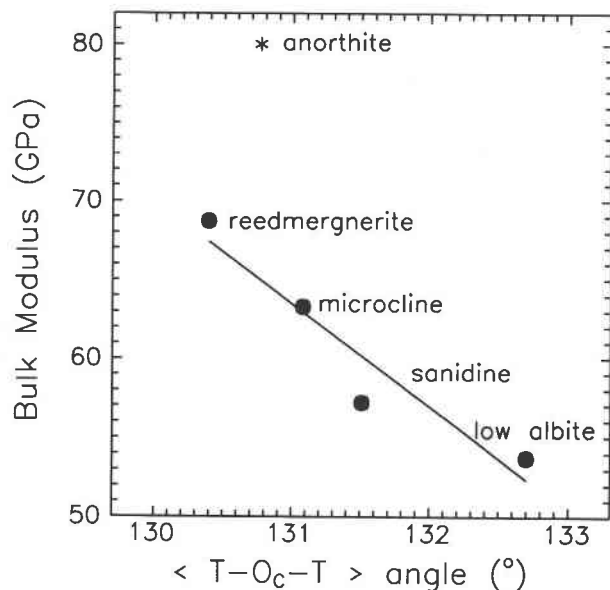


Fig. 8. The variation of the average  $T-O_c-T$  angle vs. the bulk modulus for some feldspars. The albite is from this study, and the other data points were collated by Angel (1994). Note that a correlation appears to exist for the alkali feldspars. Sanidine does not fit the trend as well as the others, perhaps reflecting structural as well as chemical disorder. However, if the data from Angel et al. (1988) for sanidine were submitted to the same Birch-Murnaghan equation of state fitting algorithm as used in this study, with weights calculated from both the errors in pressure and cell volume, then  $K_0 = 61(2)$  GPa, resulting in better agreement with the trend. Anorthite does not follow the same trend as the alkali feldspars, perhaps because of the effect of the relatively strong Ca-O bonds in influencing the direction of strain in the structure.

## DISCUSSION

A section of the albite crystal perpendicular to [010] is illustrated in Figure 3a, which shows chains of four-membered rings of tetrahedra that run parallel to [001]. These rings were called the horizontal 4-rings by Smith and Brown (1988). Compression along these chains, assuming rigid horizontal four-membered rings, would require bending of the  $Al-O_{A1}-Si$  angle. An examination of Figure 7 shows that this angle narrows only slightly with increasing pressure. Figure 3d shows that the orientation of the most compressive axis of the strain ellipsoid is perpendicular to, and more or less in, the same plane as these chains. The zigzag channels that are parallel to these chains contain the Na atoms and are a region of the crystal that is relatively weaker than other parts of the structure because of the weaker Na-O bonds. Thus it appears that compression is accomplished by narrowing the gap between the chains. Another set of chains is stacked directly below the illustrated layer, related by a symmetry inversion, and linked by the two  $O_{A2}$  atoms in each four-membered ring (Fig. 3b). Upon compression, there was little change in the distance between these layers, and the Si-

$O_{A2}-Si$  angle was observed to remain constant over the pressure interval (Fig. 7).

Another set of chains is stacked above the zigzag channels (Fig. 3c) related to the lower layer (Fig. 3a) by the C-lattice translation and linked to it by the four  $O_{CO}$  and  $O_{cm}$  atoms in each horizontal four-membered ring. An examination of Figure 7 shows that the  $Al-O_{CO}-Si$  angle undergoes significant narrowing, whereas  $Si-O_{cm}-Si$  increases slightly, if at all. This behavior is consistent with that expected from softer Al-O-Si angles and stiffer Si-O-Si angles. The  $Al-O_{CO}-Si$  and  $Si-O_{cm}-Si$  angles link the horizontal four-membered rings of the two layers into double-crankshaft chains that run parallel to [100]. Thus it appears that pressure causes the crankshaft chains to fold up, somewhat like an accordion. Interestingly, correlations of the length of the *a* axis with M-cation radius also demonstrate the flexibility of the crankshaft chains (Smith and Brown, 1988).

Internally, the horizontal four-membered ring undergoes a slight shear, with the  $O_{DO}-O_{Dm}$  separation decreasing by 0.11 Å and the  $O_{BO}-O_{Bm}$  separation increasing by 0.05 Å over the range 0–3.78 GPa. An examination of Figure 7 indicates that the  $Al-O_{DO}-Si$  and  $Si-O_{Dm}-Si$  angles widen slightly, and the  $Al-O_{BO}-Si$  angle decreases with pressure, concomitant with this shear. Essentially all the compression along the *c* axis is accommodated by this shear, with the  $T1O-T1m$  distance decreasing by 0.07 Å and the  $T2O-T2m$  distance increasing by 0.01 Å over the range 0–3.78 GPa.

To determine the structural elements that control compression, we first compared the distance between the chains of four-membered rings [this distance is the spacing of (100)] with the bulk modulus for various feldspar types: anorthite, microcline, sanidine, reedmergnerite (Angel, 1988, 1994; Angel et al., 1988; Hackwell and Angel, 1992), and low albite from this study. We anticipated that compressibility would be greatest for the structures with the largest separation between the chains. However, no discernible correlation was observed. The other obvious possibility was to compare the value of the  $Al-O_{CO}-Si$  angle for a given structure with its bulk modulus. However, since Al-Si disorder is such a common feature in feldspar structures, we made a plot of the average  $T-O_c-T$  angle vs. bulk modulus (Fig. 8). A discernible correlation seems to exist between this angle and bulk modulus, but it only holds for the alkali feldspars: the wider the angle, the more compressible the structure. From the point of view of energetics, this makes sense because the narrower the T-O-T angle, the more energy is needed to compress the angle even further. This trend is also consistent with the stiffening of the major axis of the unit-strain ellipsoid with pressure (Fig. 2). Anorthite does not follow the trend of the alkali feldspars, perhaps because of the strength of the Ca-O bonds and their influences on the compression mechanism. The strain ellipsoid for anorthite is significantly different from those in the alkali feldspars—a feature that Angel (1994) attributed to the influence of strong Ca-O bonds.

### THE EFFECT OF PRESSURE ON THE ORDERING OF ALBITE

Low albite is the common natural form of albite, with Al ordered into the T1O site. Attempts to synthesize low albite at room pressure have always failed, with only the disordered form being created. However, Martin (1969) and Goldsmith and Jenkins (1985) have shown that low albite can be synthesized from albitic glass or even from high albite at 300–400 °C and ~1–2 GPa. Having demonstrated the role of the Al-O<sub>c</sub>-Si angle in the compression of low albite, it follows that if Si disorders into the T1O site, then the T-O<sub>co</sub>-T angle will be stiffer and the compressibility of the structure decreased. The energy term,  $P\Delta V$ , will be smaller for disordered albite than for ordered albite, and so with enough heat to aid the kinetics, and with the application of pressure, Al-Si ordering is encouraged. On the other hand, since molecular orbital calculations have shown that the B-O-Si angle force constant [33.90 kcal/(mol·rad<sup>2</sup>)] is twice as large as the Si-O-Si force constant (Nicholas et al., 1992), then the opposite behavior might be observed for reedmergnerite, with B-Si disordering encouraged with increasing pressure. A possible problem, however, is that the potential well for the B-O-Si angle is relatively narrow, and therefore only a small range of angles near 130° is stable (Geisinger et al., 1985). This restricted range of angles may exclude the T-O<sub>bm</sub>-T and T-O<sub>dm</sub>-T angles (Fig. 7) and therefore excludes B from the T1m, T2O, and T2m sites. To the best of our knowledge, this experiment has not been completed; however, it could verify the ideas presented in this paper.

Goldsmith (1986) demonstrated that H plays an important role in promoting Al-Si interdiffusion in albite at high pressures—a result that may be explained qualitatively by our data. The Na-O<sub>co</sub> bond length is the longest of all the Na-O bonds to O atoms involved in Al-O-Si angles (Fig. 5), and so it follows that the O<sub>co</sub> atom is the most underbonded O atom in the albite structure. Any H present would most certainly be attracted to this site. Given the pivotal role of the O<sub>co</sub> atom when the structure is subjected to pressure, it follows that the Al-O<sub>co</sub>-Si angle would be under considerable strain. This strain, coupled with the effects of H bonding, may weaken the structure in that region. Bond breaking could easily be followed by cation diffusion. This idea could be verified through an electron density study of the albite structure in the region of the O<sub>co</sub> atom.

The results of this study demonstrate the pivotal role of the T-O<sub>c</sub>-T angle in the high-pressure behavior of alkali feldspars in general and of low albite in particular. The Al-O<sub>bo</sub>-Si angle also shows considerable narrowing with pressure, but it is not clear how primary this change is. Certainly, in a structure as complex as that of low albite, all the pressure behavior cannot be ascribed to one simple component of the structure. Computer modeling of the feldspar structure and its pressure behavior would be particularly useful, with special attention directed to

these two angles. Also, more data about the effects of pressure on the degree of Al-Si order for other feldspar structures completed in dry conditions, similar to the experiments reported by Goldsmith and Jenkins (1985), could reveal much about the Al-Si ordering mechanism.

### ACKNOWLEDGMENTS

Discussions with Ross Angel, Paul Ribbe, and Bob Martin were invaluable, and their input to this paper is gratefully acknowledged. The X-ray diffraction work and postdoctoral fellowship to R.T.D. at the Geophysical Laboratory is supported by NSF grant EAR-9218845 and the Carnegie Institution of Washington. Figure 3 was constructed with the help of Kurt Bartelmehs.

### REFERENCES CITED

- Abrahams, S.C., and Keve, E.T. (1971) Normal probability plot analysis of error in measured and derived quantities and standard deviations. *Acta Crystallographica*, A27, 157–165.
- Angel, R.J. (1988) High-pressure structure of anorthite. *American Mineralogist*, 73, 1114–1119.
- (1994) Feldspars at high pressure. In I. Parsons, Ed., *Feldspars and their reactions*, NATO ASI series C, Mathematical and Physical Sciences, p. 271–312. Kluwer Academic, Dordrecht, The Netherlands.
- Angel, R.J., Hazen, R.M., McCormick, T.C., Prewitt, C.T., and Smyth, J.R. (1988) Comparative compressibility of end-member feldspars. *Physics and Chemistry of Minerals*, 15, 313–318.
- Armbruster, T., Bürgi, H.B., Kunz, M., Gnos, E., Brönnimann, S., and Lienert, C. (1990) Variation of displacement parameters in structure refinements of low albite. *American Mineralogist*, 75, 135–140.
- Becker, P.J., and Coppens, P. (1975) Extinction within the limit of validity of the Darwin transfer equations: III. Non-spherical crystals and anisotropy of extinction. *Acta Crystallographica*, A31, 417–425.
- Daniel, I., Gillet, P., and McMillan, P. (1993) A Raman spectroscopic study of CaAl<sub>2</sub>Si<sub>2</sub>O<sub>8</sub> at high-pressure and high-temperature: Polymorphism, melting and amorphization (abs.), p. 10. Nato Advanced Study Institute, Edinburgh, Scotland.
- Downs, R.T., and Palmer, D.C. (1994) The pressure behavior of  $\alpha$  cristobalite. *American Mineralogist*, 79, 9–14.
- Doyle, P.A., and Turner, P.S. (1968) Relativistic Hartree-Fock X-ray and electron scattering factors. *Acta Crystallographica*, A24, 390–397.
- Finger, L.W., and Prince, E. (1975) A system of Fortran IV computer programs for crystal structure computations, 128 p. U.S. National Bureau of Standards, Technical Note 854.
- Geisinger, K.L., Gibbs, G.V., and Navrotsky, A. (1985) A molecular orbital study of bond length and angle variations in framework structures. *Physics and Chemistry of Minerals*, 11, 266–283.
- Giletti, B.J., Semet, M.P., and Yund, R.A. (1978) Studies in diffusion: III. Oxygen in feldspars: An ion microprobe determination. *Geochimica et Cosmochimica Acta*, 42, 45–57.
- Glinnemann, J., King, H.E., Jr., Schulz, H., Hahn, Th., La Placa, S.J., and Dacol, F. (1992) Crystal structures of the low temperature quartz type phases of SiO<sub>2</sub> and GeO<sub>2</sub> at elevated pressure. *Zeitschrift für Kristallographie*, 198, 177–212.
- Goldsmith, J.R. (1986) The role of hydrogen in promoting Al-Si interdiffusion in albite (NaAlSi<sub>3</sub>O<sub>8</sub>) at high pressures. *Earth and Planetary Science Letters*, 80, 135–138.
- Goldsmith, J.R., and Jenkins, D.M. (1985) The high-low albite relations revealed by reversal of degree of order at high pressures. *American Mineralogist*, 70, 911–923.
- Hackwell, T.P. (1993) *Feldspars at high pressures and temperatures*. Ph.D. dissertation, University College London, London.
- Hackwell, T.P., and Angel, R.J. (1992) The comparative compressibility of reedmergnerite, danburite and their aluminum analogues. *European Journal of Mineralogy*, 4, 1221–1227.
- Harlow, G.E., and Brown, G.E., Jr. (1980) Low albite: An X-ray and neutron diffraction study. *American Mineralogist*, 65, 986–995.
- Hazen, R.M., and Finger, L.W. (1982) *Comparative crystal chemistry*, 231 p. Wiley, New York.

- Hazen, R.M., and Prewitt, C.T. (1977) Linear compressibilities of low albite: High-pressure structural implications. *American Mineralogist*, 62, 554–558.
- Hazen, R.M., Finger, L.W., Hemley, R.J., and Mao, H.K. (1989) High-pressure crystal chemistry and amorphization of  $\alpha$ -quartz. *Solid State Communications*, 72, 507–511.
- Holland, T.J.B. (1980) The reaction albite = jadeite + quartz determined experimentally in the range 600–1200 °C. *American Mineralogist*, 65, 129–134.
- Ibers, J.A., and Hamilton, W.C., Eds. (1974) *International tables for X-ray crystallography*, vol. IV, 366 p. Kynoch, Birmingham, U.K.
- King, H.E., and Finger, L.W. (1979) Diffracted beam crystal centering and its application to high-pressure crystallography. *Journal of Applied Crystallography*, 12, 374–378.
- Kroll, H. (1983) Lattice parameters and determinative methods for plagioclase and ternary feldspars. In *Mineralogical Society of America Reviews in Mineralogy*, 2, 101–119.
- Kroll, H., and Ribbe, P.H. (1980) Determinative diagrams for Al,Si order in plagioclases. *American Mineralogist*, 65, 449–457.
- Levien, L., and Prewitt, C.T. (1981) High-pressure crystal structure and compressibility of coesite. *American Mineralogist*, 66, 324–333.
- Mao, H.K., Bell, P.M., Shaner, J.W., and Steinberg, D.J. (1978) Specific volume measurements of Cu, Mo, Pd, and Ag and calibration of the ruby R, fluorescence pressure gauge from 0.06 to 1 Mbar. *The Journal of Applied Physics*, 49, 3276–3283.
- Martin, R.F. (1969) The hydrothermal synthesis of low albite. *Contributions to Mineralogy and Petrology*, 23, 323–339.
- Merrill, L., and Bassett, W.A. (1974) Miniature diamond anvil pressure cell for single crystal X-ray diffraction studies. *Review of Scientific Instruments*, 45, 290–294.
- Nicholas, J.B., Winans, R.E., Harrison, R.J., Iton, L.E., Curtiss, L.A., and Hopfinger, A.J. (1992) Ab initio molecular orbital study of the effects of basis set size on the calculated structure and acidity of hydroxyl groups in framework molecular sieves. *The Journal of Physical Chemistry*, 96, 10247–10257.
- Robinson, K., Gibbs, G.V., and Ribbe, P.H. (1971) Quadratic elongation: A quantitative measure of distortion in coordinated polyhedra. *Science*, 172, 567–570.
- Smith, J.V., and Brown, W.L. (1988) *Feldspar minerals: I. Crystal structures, physical, chemical, and microtextural properties*, 828 p. Springer-Verlag, New York.
- Smith, J.V., Artioli, G., and Kvick, Å. (1986) Low albite, NaAlSi<sub>3</sub>O<sub>8</sub>: Neutron diffraction study of crystal structure at 13 K. *American Mineralogist*, 71, 727–733.
- Wainwright, J.E., and Starkey, J. (1968) Crystal structure of a metamorphic low albite. Program of the November 11–13, 1968, Geological Society Annual Meeting, Mexico City, 310.
- Wenk, H.R., and Kroll, H. (1984) Analysis of  $P\bar{1}$ ,  $I\bar{1}$ , and  $C\bar{1}$  plagioclase structures. *Bulletin de Minéralogie*, 107, 467–487.
- Williams, Q., and Jeanloz, R. (1989) Static amorphization of anorthite at 300 K and comparison with diaplectic glass. *Nature*, 338, 413–415.
- Winter, J.K., Ghose, S., and Okamura, F.P. (1977) A high-temperature study of the thermal expansion and the anisotropy of the sodium atom in low albite. *American Mineralogist*, 62, 921–931.
- Yoder, H.S., and Weir, C.E. (1951) Change of free energy with pressure of the reaction nepheline + albite = 2 jadeite. *American Journal of Science*, 249, 683–694.

MANUSCRIPT RECEIVED APRIL 13, 1994

MANUSCRIPT ACCEPTED JULY 7, 1994